

Minimum Description Length based Granular-Ball Tree Regularization for Spectral Clustering

Zeqiang Xian^{a,b,1}, Caihui Liu^{a,b,*}, Yong Zhang^{a,b}, Wenjing Qiu^{a,b}

^a*Department of Mathematics and Computer Science, Gannan Normal
University, Ganzhou, 341000, Jiangxi, China*

^b*Key Laboratory of Data Science and Artificial Intelligence of Jiangxi Education Institutes, Gannan
Normal University, Ganzhou, 341000, Jiangxi, China*

Abstract

Spectral clustering largely depends on the affinity graph, yet constructing a graph that preserves reliable local connectivity while adapting to heterogeneous data structures remains challenging. Existing granular-ball-based spectral clustering methods usually reduce graph complexity by using coarse-grained representatives. However, the learned local regions are often treated as graph nodes or anchors, and their structural information is not sufficiently used to regularize the original sample-level graph. To address this issue, this paper proposes a Minimum Description Length based Granular-Ball Tree-Regularized Spectral Clustering method, termed MDL-GBTRSC. The proposed method constructs a granular-ball tree through local MDL model selection, with reciprocal neighborhood continuity used to discourage splits that break reliable local connections. The stable leaf balls obtained from the tree provide coding-scale information for regularizing the sample-level affinity graph. In addition, a shared-neighbor bridge code is introduced to adjust weak local bridge relations without requiring an additional user-specified threshold. In this way, MDL-GBTRSC connects interpretable local representation learning with affinity graph construction in a unified spectral clustering framework. Experiments on real and synthetic datasets show that MDL-GBTRSC achieves the best average ARI and NMI under the adopted fixed-configuration protocol compared with classical spectral clustering baselines and representative granular-ball, micro-cluster, and anchor-based methods.

Keywords: spectral clustering, granular-ball computing, minimum description length, affinity graph construction, non-parametric clustering

1. Introduction

Clustering is a fundamental task in unsupervised learning and data mining, aiming to reveal the intrinsic organization of unlabeled data [1]. Among various clustering methods, spectral clustering transforms clustering into a graph partitioning problem and is able to handle non-convex structures that are difficult for centroid-based methods to describe [2, 3, 4]. In spectral clustering, data samples are represented as vertices in

*Corresponding author.

Email addresses: xianzeqiang@gnnu.edu.cn (Zeqiang Xian), liucaihui@gnnu.edu.cn (Caihui Liu), zhang_yong@gnnu.edu.cn (Yong Zhang), wenjingqiu@gnnu.edu.cn (Wenjing Qiu)

¹The first author contributed to this work.

a weighted graph, and the clustering result is obtained from the spectral embedding induced by the graph Laplacian. Therefore, the affinity graph is not only an intermediate representation. It directly affects which local relations are preserved, propagated, or separated during clustering.

Despite its effectiveness, spectral clustering remains sensitive to graph construction. Classical strategies, such as k -nearest-neighbor graphs and RBF graphs, usually depend on a fixed neighborhood order or kernel scale. Such predefined graph scales may be insufficient when the data contain heterogeneous densities, weak boundaries, noisy local connections, or curved cluster structures. To improve graph adaptability, graph structure learning has been systematically studied in recent years [5]. Direct spectral clustering [6] reduces the separation between graph construction and clustering assignment. Structured doubly stochastic graph-based clustering [7] learns graphs that are more consistent with cluster indicators. Stacked adaptive graph learning [8] refines graph relations through latent representations. These studies indicate that the graph used for spectral clustering should be consistent with the local structure of data rather than being determined only by a predefined pairwise rule.

Graph construction is also closely related to scalability. Classical spectral clustering requires an affinity matrix over all samples and eigendecomposition of the graph Laplacian, which becomes expensive as the sample size increases. Anchor-based and bipartite-graph-based methods reduce this cost by constructing relations between samples and representative anchors. Self-adapted bipartite graph learning [9] learns a bipartite graph and a low-dimensional representation, while discrete and balanced spectral clustering [10] combines anchor representation with discrete partition learning. Spectral clustering with linear embedding [11] directly solves the cluster indicator matrix in a scalable formulation, and approximate spectral embedding representation [12] estimates sample embeddings from representative anchors. Recent GMM-enhanced anchor-based spectral clustering [13] further considers membership heterogeneity by distinguishing prior-consistent and prior-uncertain samples. These methods reduce the computational burden of spectral clustering, but their performance still depends on whether the representative structure preserves meaningful local geometry and connectivity.

Another line of studies improves affinity construction by incorporating local structural assumptions. Subspace-distance based spectral clustering [14] measures local subspace relations for similarity construction. Diffusion-based affinity learning [15] refines pairwise similarities through neighborhood propagation. For data with heterogeneous densities, stratified multi-density spectral clustering [16] uses Gaussian mixture modeling and density stratification to adjust the adjacency matrix. These methods show that graph construction can benefit from local structural information. However, they mainly learn or adjust pairwise similarities directly. How to introduce interpretable local region-level information into the affinity graph without relying mainly on manually selected graph scales remains a challenging problem.

Granular-ball computing provides a local-region representation for addressing this problem. Instead of treating each sample as an isolated computational unit, granular-ball computing represents data by adaptive local regions, each usually characterized by its center, radius, and covered samples [17, 18]. This representation is naturally multi-granular. Simple regions can be summarized by coarse balls, whereas structurally complex regions can be refined into smaller ones. In clustering, GBCT [19] models relations among granular balls to obtain cluster structures. In spectral clustering,

GBSC [20] constructs the similarity matrix on granular balls instead of all original samples. Granular-ball computing-based manifold clustering [21] treats granular balls as adaptive anchors, and pseudo-label-based granular-ball division [22] uses pseudo-purity to generate anchor points for large-scale spectral clustering. Related micro-cluster based methods, such as MDMSC [23], also indicate that local density and manifold structure can help construct representative regions before spectral partitioning.

Although these methods demonstrate the value of local region-level representations, most granular-ball or micro-cluster based spectral clustering methods mainly use the generated regions as reduced graph nodes, anchors, or intermediate representatives. In this setting, granular balls usually serve to reduce the graph scale or simplify the subsequent spectral clustering problem. The structural information contained in the generated regions, such as local scale, dispersion, and reliability, is not sufficiently fed back into the original sample-level affinity graph. Consequently, local region generation and final graph construction remain relatively separated. In addition, many granular-ball generation strategies depend on compactness measures, density rules, pseudo-label purity, or heuristic splitting criteria. These criteria can be effective in practice, but the retain-or-split decision is not always formulated under a unified and interpretable objective.

The Minimum Description Length (MDL) principle provides a model-selection perspective for local region construction. Under the MDL principle, a local structure is preferred when it provides a shorter description of the samples it covers. Recent MDL-based granular-ball generation has shown that granular-ball construction can be formulated as a competition among alternative local explanations [24]. Boundary-aware MDL granular-ball classification further indicates that MDL-based local modeling can be extended from unsupervised representation to supervised decision boundaries [25]. These studies suggest that MDL can provide an interpretable criterion for local granular-ball construction. For spectral clustering, this view is particularly relevant because an MDL-induced granular-ball structure can provide adaptive coding-scale information for affinity graph construction, rather than only serving as a reduced representation.

Motivated by the above observations, this paper proposes a Minimum Description Length based Granular-Ball Tree-Regularized Spectral Clustering method, abbreviated as MDL-GBTRSC. The proposed method constructs an MDL-induced granular-ball tree and uses its stable leaf balls to regularize the sample-level affinity graph. Specifically, a reciprocal preliminary graph is first constructed to describe reliable neighborhood continuity. During tree construction, candidate splits are evaluated according to both local description-length reduction and the cost of cutting reciprocal neighborhood relations. After the tree is obtained, the stable leaf balls provide coding-scale information for the final affinity graph. A shared-neighbor bridge code is further introduced under a component-count condition to adjust weak local bridge relations without requiring an additional user-specified threshold.

The main distinction of MDL-GBTRSC is that granular balls are not used only to replace samples or serve as anchors. Instead, the learned granular-ball tree transfers local structural information back to the sample-level graph. The reciprocal preliminary graph regularizes tree construction by discouraging splits that break strongly supported local continuity. The stable leaf balls then regularize final graph construction through adaptive coding scales. As a result, the final graph incorporates sample-level neighborhood relations, local bridge support, and granular-ball-level structural information within a unified framework.

The main contributions of this paper are summarized as follows.

- A Minimum Description Length based Granular-Ball Tree-Regularized Spectral Clustering method is proposed. The learned granular-ball tree is used to regularize the sample-level affinity graph, rather than simply replacing samples with granular-ball centers or anchors.
- A graph-continuity regularized MDL criterion is developed for granular-ball tree construction. Candidate splits are evaluated according to both description-length reduction and their influence on reciprocal neighborhood continuity, so that local representation learning and neighborhood preservation are considered in a unified criterion.
- A tree-regularized affinity construction mechanism is introduced. Stable leaf balls provide adaptive coding scales for the final affinity graph, while the shared-neighbor bridge code assigns additional description length to edges with limited common-neighborhood support under a component-count condition, reducing weak bridge affinities without introducing an additional user-specified threshold.
- Experiments on synthetic and real benchmark datasets evaluate the effectiveness of MDL-GBTRSC. The results show that the proposed method can achieve competitive clustering performance on non-convex synthetic structures and real-world clustering tasks.

The remainder of this paper is organized as follows. Section 2 presents the proposed MDL-GBTRSC method. Section 3 analyzes its computational complexity. Section 4 reports the experimental results. Finally, Section 5 concludes this paper.

2. Methodology

This section presents the proposed Minimum Description Length based Granular-Ball Tree-Regularized Spectral Clustering method, abbreviated as MDL-GBTRSC. The method constructs an affinity graph by combining local granular-ball representation with neighborhood continuity. Instead of applying spectral clustering directly to a graph defined only by pairwise distances, MDL-GBTRSC first learns a granular-ball tree under a local MDL criterion and then uses the stable leaf balls to regularize the final affinity graph.

The main idea is that granular balls and graph affinities describe complementary aspects of data structure. Granular balls provide compact local descriptions, while graph affinities preserve neighborhood connectivity and are useful for non-convex clusters. In MDL-GBTRSC, a reciprocal neighborhood graph supplies local continuity evidence during tree construction. A candidate split is accepted only when its reduction in representation cost is sufficient to compensate for the description cost caused by cutting reciprocal neighborhood relations. After the tree is obtained, the stable leaf balls provide local coding scales for graph construction. The final partition is obtained either from connected components or by spectral clustering on the selected tree-regularized graph.

2.1. Problem Formulation

Let $X = \{x_1, x_2, \dots, x_n\}$ be an unlabeled dataset, where $x_i \in \mathbb{R}^d$. The clustering task is to obtain a K -way partition $\Pi = \{C_1, C_2, \dots, C_K\}$. In the fixed- K setting, K is provided as input. When K is not specified, it can be estimated from the learned graph by an eigengap rule. For clustering problems considered in this paper, $n \geq 2$ is assumed.

Before model construction, each feature is linearly normalized into $[0, 1]$:

$$x'_{ij} = \frac{x_{ij} - \min(x_{.j})}{\max(x_{.j}) - \min(x_{.j})}, \quad j = 1, 2, \dots, d. \quad (1)$$

For a constant feature, all normalized values are set to zero. For simplicity, the normalized dataset is still denoted by X .

2.2. Reciprocal Neighborhood Continuity

A preliminary neighborhood graph is constructed before granular-ball generation. This graph is not used directly as the final clustering graph. Its role is to provide local continuity evidence when evaluating whether a candidate split preserves or breaks neighborhood relations.

The neighborhood order is determined by the sample size and feature dimension:

$$k_g = \min \left\{ n - 1, \max \left(2, \left\lceil \log_2(n + 1) + \sqrt{d} \right\rceil \right) \right\}. \quad (2)$$

Let $N_g(i)$ denote the k_g -nearest-neighbor set of x_i , and let $d_i^{(g)}$ be the distance from x_i to its k_g -th nearest neighbor. The local scale of x_i is defined as $\tilde{\tau}_i = \max\{d_i^{(g)}, \epsilon\}$. For a directed neighboring pair $j \in N_g(i)$, the self-tuning affinity is

$$\bar{a}_{ij} = \exp \left(-\frac{\|x_i - x_j\|_2^2}{2\tilde{\tau}_i\tilde{\tau}_j} \right), \quad (3)$$

and $\bar{a}_{ij} = 0$ if $j \notin N_g(i)$.

A reciprocal relation is retained only when two samples are mutual neighbors. The reciprocal preliminary affinity is

$$a_{ij}^{\text{rec}} = \begin{cases} \min\{\bar{a}_{ij}, \bar{a}_{ji}\}, & j \in N_g(i) \text{ and } i \in N_g(j), \\ 0, & \text{otherwise.} \end{cases} \quad (4)$$

The resulting reciprocal graph is denoted by G_{rec}^0 . Its edge set E_{rec}^0 is treated as an undirected edge set and consists of all pairs with $a_{ij}^{\text{rec}} > 0$.

Property 1 (Range and reciprocity). *For any reciprocal neighboring pair (i, j) , $0 < a_{ij}^{\text{rec}} \leq 1$ and $a_{ij}^{\text{rec}} = a_{ji}^{\text{rec}}$.*

Proof 1. *Since $\tilde{\tau}_i > 0$ and $\tilde{\tau}_j > 0$, the directed affinity in Eq. (3) belongs to $(0, 1]$ whenever the directed relation exists. For a reciprocal pair, both \bar{a}_{ij} and \bar{a}_{ji} are positive, and their minimum is also in $(0, 1]$. The definition in Eq. (4) is symmetric in i and j , so $a_{ij}^{\text{rec}} = a_{ji}^{\text{rec}}$.*

2.3. Granular-Ball Coding

For a granular ball $B \subseteq X$, let I_B be its index set and $n_B = |I_B|$. Its empirical center, residual sum of squares, and radius are defined as

$$c_B = \frac{1}{n_B} \sum_{i \in I_B} x_i, \quad \text{SSE}(B) = \sum_{i \in I_B} \|x_i - c_B\|_2^2, \quad r_B = \max_{i \in I_B} \|x_i - c_B\|_2. \quad (5)$$

A finite-resolution variance floor is estimated by

$$\sigma_{\min}^2 = \max \left\{ \frac{\text{median}_i \left[(d_i^{(1)})^2 \right]}{d}, \epsilon \right\}, \quad (6)$$

where $d_i^{(1)}$ is the first-nearest-neighbor distance of x_i . The effective variance of B is

$$\tilde{\sigma}_B^2 = \max \left\{ \frac{\text{SSE}(B)}{n_B d}, \sigma_{\min}^2 \right\}. \quad (7)$$

2.3.1. Isotropic ball code

The isotropic model locally describes the samples in B by $x_i \sim \mathcal{N}(c_B, \sigma_B^2 I_d)$. This is used as a local coding model rather than as a global distributional assumption. With the finite-resolution variance floor, the isotropic description length is

$$L_{\text{iso}}(B) = \frac{n_B d}{2} [\log(2\pi) + 1 + \log(\tilde{\sigma}_B^2)] + \frac{d+1}{2} \log \max\{n_B, 2\}. \quad (8)$$

The likelihood part follows from the Gaussian maximum likelihood estimates of the center and variance before applying the variance floor, while the complexity term corresponds to d center parameters and one variance parameter.

Proposition 1 (Closed-form isotropic code). *Under the isotropic Gaussian coding model, before applying the finite-resolution variance floor, the empirical mean and empirical variance minimize the negative log-likelihood. Substituting these estimates yields the likelihood part of Eq. (8).*

Proof 2. *For fixed variance, minimizing the negative log-likelihood is equivalent to minimizing $\sum_{i \in I_B} \|x_i - c_B\|_2^2$, whose minimizer is the empirical mean. For the fixed empirical mean, differentiating the negative log-likelihood with respect to σ_B^2 gives the empirical variance. Substituting these estimates gives the stated likelihood term. The variance floor in Eq. (7) is then applied to keep the logarithmic term well-defined.*

2.3.2. Subspace-adaptive ball code

For anisotropic local regions, a subspace-adaptive code is also evaluated. Let

$$M_B = \sum_{i \in I_B} (x_i - c_B)(x_i - c_B)^\top \quad (9)$$

be the unnormalized local scatter matrix, and let $\lambda_1 \geq \lambda_2 \geq \dots \geq \lambda_d \geq 0$ be its eigenvalues. For an intrinsic dimension candidate $q \in \{0, 1, \dots, d\}$, the data code is divided into a parallel part and an orthogonal part.

For $q > 0$, the variance in the parallel subspace is

$$\tilde{\sigma}_{\parallel,q}^2 = \max \left\{ \frac{\sum_{\ell=1}^q \lambda_\ell}{n_B q}, \sigma_{\min}^2 \right\}, \quad (10)$$

and for $q < d$, the variance in the orthogonal complement is

$$\tilde{\sigma}_{\perp,q}^2 = \max \left\{ \frac{\sum_{\ell=q+1}^d \lambda_\ell}{n_B(d-q)}, \sigma_{\min}^2 \right\}. \quad (11)$$

The corresponding data codes are

$$\Psi_{\parallel}(B, q) = \begin{cases} \frac{n_B q}{2} [\log(2\pi) + 1 + \log(\tilde{\sigma}_{\parallel,q}^2)], & q > 0, \\ 0, & q = 0, \end{cases} \quad (12)$$

and

$$\Psi_{\perp}(B, q) = \begin{cases} \frac{n_B(d-q)}{2} [\log(2\pi) + 1 + \log(\tilde{\sigma}_{\perp,q}^2)], & q < d, \\ 0, & q = d. \end{cases} \quad (13)$$

The subspace-adaptive description length is

$$L_{\text{sub}}(B, q) = \Psi_{\parallel}(B, q) + \Psi_{\perp}(B, q) + \frac{k_{\text{sub}}(q)}{2} \log \max\{n_B, 2\} + \log(d+1), \quad (14)$$

where

$$k_{\text{sub}}(q) = d + \mathbb{I}(q > 0) + \mathbb{I}(d - q > 0) + q(d - q). \quad (15)$$

Here $\mathbb{I}(\cdot)$ denotes the indicator function, which equals one if the condition is satisfied and zero otherwise. The term d corresponds to the ball center, the two indicator terms correspond to the required variance components, and $q(d - q)$ accounts for the degrees of freedom of a q -dimensional subspace in \mathbb{R}^d . The term $\log(d+1)$ encodes the selection of q .

The best subspace-adaptive code is

$$L_{\text{sub}}(B) = \min_{0 \leq q \leq d} L_{\text{sub}}(B, q). \quad (16)$$

For $d > 1$, the leaf-ball description length is

$$L_{\text{leaf}}(B) = \min \{L_{\text{iso}}(B), L_{\text{sub}}(B)\} + \log 2. \quad (17)$$

The term $\log 2$ encodes the representation choice between the isotropic and subspace-adaptive descriptions. When $d = 1$, no nontrivial subspace decomposition is needed, and the isotropic code is used directly.

Proposition 2 (Two-part form of the leaf-ball code). *For $d > 1$, the leaf-ball code in Eq. (17) is a two-part MDL code: it first encodes the selected representation type and then encodes the samples under that representation.*

Proof 3. *There are two representation candidates. A uniform model-index code requires $\log 2$ nats to encode the selected candidate. Once the representation is specified, the samples are encoded by the corresponding description length. Taking the shorter data code and adding the representation-index cost gives Eq. (17).*

2.4. Graph-Regularized Granular-Ball Tree

The granular-ball tree starts from the root ball containing all samples. For a current ball B , two local explanations are compared: retaining B as a stable ball or splitting it into two child balls. The decision is made by a local MDL criterion regularized by the reciprocal preliminary graph.

2.4.1. Admissible granularity

To avoid degenerate child balls, the minimum admissible child size is defined as

$$n_{\min}(B) = \begin{cases} 1, & n_B \leq 3, \\ \min \left\{ \left\lfloor \frac{n_B}{2} \right\rfloor, \max \left[2, \left\lceil \min \left(\frac{\sqrt{n_B}}{\log \sqrt{d+2}}, d+2 \right) \right\rceil \right] \right\}, & n_B > 3. \end{cases} \quad (18)$$

A split $B \rightarrow (B_L, B_R)$ is admissible if $n_{B_L} \geq n_{\min}(B)$ and $n_{B_R} \geq n_{\min}(B)$. For $n_B > 3$, Eq. (18) gives $2 \leq n_{\min}(B) \leq \lfloor n_B/2 \rfloor$, so an admissible split, when considered, can produce two non-empty child balls.

2.4.2. Local MDL decision

If B is retained, its description length is

$$L_1(B) = L_{\text{leaf}}(B) + \log 2, \quad (19)$$

where the additional $\log 2$ encodes the structural choice between retaining and splitting.

For a generated split candidate $B \rightarrow (B_L, B_R)$, the split description length is

$$\ell_2(B_L, B_R) = L_{\text{leaf}}(B_L) + L_{\text{leaf}}(B_R) + L_{\text{cut}}(B_L, B_R) + \log 2 + \log(|Q_B| + 1). \quad (20)$$

Here R_B denotes the finite set of deterministic candidate orderings. For each ordering, admissible cut positions are determined by the minimum child-size constraint in Eq. (18). The set Q_B denotes the admissible ordering-position pairs generated from these orderings. Once an ordering-position pair is specified, the two child balls are determined, so no additional arbitrary subset-membership code is required.

The graph-continuity cut code is

$$L_{\text{cut}}(B_L, B_R) = \sum_{\substack{i \in B_L, j \in B_R \\ \{i, j\} \in E_{\text{rec}}^0}} -\log(\max\{1 - a_{ij}^{\text{rec}}, \epsilon\}). \quad (21)$$

Since E_{rec}^0 is undirected, each separated reciprocal edge is counted once. This term assigns a larger cost to a split that separates strongly connected reciprocal neighboring samples. Therefore, a split is accepted only when its reduction in local representation cost is sufficient to compensate for the loss of reciprocal neighborhood continuity.

Let S_B be the deterministic set of generated admissible split candidates selected from Q_B . The best generated split code is

$$L_2(B) = \min_{(B_L, B_R) \in S_B} \ell_2(B_L, B_R), \quad (22)$$

where $L_2(B) = +\infty$ if S_B is empty. The MDL gain is

$$\Delta(B) = L_1(B) - L_2(B). \quad (23)$$

The local decision is to split B if $\Delta(B) > 0$, and to retain B otherwise.

Property 2 (Continuity-preserving effect). For a fixed split, the separated-edge cost in Eq. (21) is non-decreasing with respect to a_{ij}^{rec} .

Proof 4. Without clipping, $f(a) = -\log(1 - a)$ satisfies $f'(a) = 1/(1 - a) > 0$ for $0 < a < 1$. With the lower bound ϵ , the cost is clipped only when $1 - a \leq \epsilon$, so the implemented cost remains non-decreasing.

Proposition 3 (Local MDL decision). The local decision selects the shorter description between retaining B and applying the best generated admissible split.

Proof 5. If $\Delta(B) > 0$, then $L_2(B) < L_1(B)$, so the generated split explanation is shorter. If $\Delta(B) \leq 0$, then $L_1(B) \leq L_2(B)$, so retaining B is no worse than applying any generated admissible split in S_B .

The tree is expanded in a best-first manner by repeatedly splitting the leaf ball with the largest positive gain. The process stops when no leaf ball has positive gain. The final stable leaf balls are denoted by $\{B_1^*, \dots, B_m^*\}$.

Theorem 1 (Finite termination). The tree construction terminates after a finite number of accepted splits.

Proof 6. Each accepted split replaces one leaf ball by two non-empty child balls, increasing the number of leaf balls by one. Since leaf balls are disjoint and each contains at least one sample, the number of leaf balls cannot exceed n . Therefore, at most $n - 1$ splits can be accepted.

2.5. Tree-Regularized Affinity Graph

After tree construction, each sample belongs to one stable leaf ball. Let $b(i)$ denote the index of the leaf ball containing x_i . For a leaf ball B_b^* , let r_b and $\tilde{\sigma}_b^2$ denote its radius and effective variance, respectively. Its coding scale is defined as

$$\eta_b = r_b + \sqrt{\tilde{\sigma}_b^2} + \epsilon. \quad (24)$$

For a directed neighboring pair $j \in N_g(i)$, the tree-regularized edge cost is

$$\phi_{ij} = \frac{\|x_i - x_j\|_2^2}{2\tilde{\tau}_i\tilde{\tau}_j} + \left| \log \frac{\eta_{b(i)}}{\eta_{b(j)}} \right|. \quad (25)$$

The corresponding directed affinity is $\bar{w}_{ij} = \exp(-\phi_{ij})$ for $j \in N_g(i)$, and $\bar{w}_{ij} = 0$ otherwise. The first term preserves local sample proximity, while the second term reduces affinity between neighboring samples whose leaf balls have substantially different local coding scales.

Two graph descriptions are derived from the directed affinities. The reciprocal affinity keeps only bidirectionally supported relations:

$$\bar{w}_{ij}^{\text{rec}} = \begin{cases} \min\{\bar{w}_{ij}, \bar{w}_{ji}\}, & \bar{w}_{ij} > 0 \text{ and } \bar{w}_{ji} > 0, \\ 0, & \text{otherwise.} \end{cases} \quad (26)$$

The completed affinity is $\bar{w}_{ij}^{\text{com}} = \max\{\bar{w}_{ij}, \bar{w}_{ji}\}$. The reciprocal graph is stricter, while the completed graph restores one-sided but locally coded relations.

Let $\kappa(W)$ denote the number of connected components induced by the nonzero entries of W . In the fixed- K setting, the shared-neighbor bridge adjustment is activated when the reciprocal and completed graphs have the same number of connected components and this number is smaller than K :

$$\delta_{\text{br}} = \mathbb{I} \{ \kappa(\bar{W}^{\text{rec}}) = \kappa(\bar{W}^{\text{com}}) < K \}. \quad (27)$$

When K is not specified, $\delta_{\text{br}} = 0$. This component-count condition is determined by the learned graph structure and the specified cluster number, and it does not introduce an additional user-specified threshold.

For a directed neighboring pair, the common-neighborhood support is

$$\gamma_{ij} = \frac{1 + |N_g(i) \cap N_g(j)|}{k_g + 1}. \quad (28)$$

The bridge code is $L_{\text{br}}(i, j) = -\log(\max\{\gamma_{ij}, \epsilon\})$, and the final directed affinity is

$$\tilde{w}_{ij} = \exp[-\phi_{ij} - \delta_{\text{br}} L_{\text{br}}(i, j)]. \quad (29)$$

The final reciprocal and completed matrices, denoted by W^{rec} and W^{com} , are obtained by applying the same symmetrization rules to \tilde{w}_{ij} .

Property 3 (Bridge effect). *For any directed neighboring pair, $0 < \tilde{w}_{ij} \leq \bar{w}_{ij} \leq 1$ when $\delta_{\text{br}} = 1$, and $\tilde{w}_{ij} = \bar{w}_{ij}$ when $\delta_{\text{br}} = 0$.*

Proof 7. *By definition, $0 < \gamma_{ij} \leq 1$, so $L_{\text{br}}(i, j) \geq 0$. If $\delta_{\text{br}} = 1$, the final edge cost is no smaller than ϕ_{ij} , and the affinity cannot increase. If $\delta_{\text{br}} = 0$, the bridge term vanishes.*

2.6. Graph Partitioning

The final graph is selected from W^{rec} and W^{com} . If K is specified and W^{rec} contains exactly K connected components, the reciprocal graph is selected. Otherwise, the completed graph is selected. This rule uses a component partition when the reciprocal graph already provides a K -way structure, while retaining the completed graph for spectral relaxation in the remaining cases.

Let W be the selected affinity matrix. The degree matrix is $D_{ii} = \sum_j w_{ij}$, and the normalized graph Laplacian is

$$L_{\text{sym}} = I - D^{-1/2} W D^{-1/2}. \quad (30)$$

If K is not specified, it is estimated by an eigengap rule on L_{sym} .

After K is determined, the component structure of W is considered. If W contains exactly K connected components, the component labels are used directly. If W is disconnected and contains c components with $1 < c < K$, spectral relaxation is performed component-wise. Let the connected components be H_1, H_2, \dots, H_c , where $n_t = |H_t|$. Denote by K_t the number of clusters assigned to component H_t . The feasible allocation set is defined as

$$A_K = \left\{ (K_1, \dots, K_c) : K_t \in \{1, \dots, n_t\}, t = 1, \dots, c, \sum_{t=1}^c K_t = K \right\}. \quad (31)$$

The component-wise cluster allocation is determined by

$$(K_1^*, \dots, K_c^*) \in \arg \min_{(K_1, \dots, K_c) \in A_K} \max_{1 \leq t \leq c} \frac{n_t}{K_t}. \quad (32)$$

Spectral clustering is then applied within each component H_t using its assigned cluster number K_t^* . If W is connected, spectral clustering is applied to W as a whole. When W contains more than K connected components, spectral relaxation is also applied to the selected graph to obtain a K -way partition. This case corresponds to merging some disconnected components in the final K -way partition.

Proposition 4 (Component-consistent partition). *If the selected graph contains exactly K connected components, assigning one label to each component gives a K -way partition without cutting any edge of the selected graph.*

Proof 8. *Connected components form a disjoint cover of the vertex set. If there are exactly K components, assigning a distinct label to each component yields a K -way partition. Since no edge exists between different connected components, no selected graph edge is cut.*

2.7. Algorithmic Procedure

The complete workflow of the proposed GBTRSC framework is illustrated in Fig. 1 and summarized in Algorithm 1. MDL-GBTRSC first constructs a reciprocal preliminary graph, then grows an MDL granular-ball tree under graph-continuity regularization. The stable leaf balls are used to construct the final tree-regularized graph, on which component-based partitioning or spectral clustering is performed.

The procedure highlights the connection between tree construction and graph partitioning. The reciprocal preliminary graph regularizes local split decisions, while the learned leaf balls provide local scale information for graph construction. Consequently, the final spectral partition is performed on a graph informed by both neighborhood continuity and granular-ball-level representation.

3. Computational Complexity Analysis

This section analyzes the computational complexity of MDL-GBTRSC. Let n denote the number of samples, d denote the feature dimension, and k_g denote the neighborhood order defined in Eq. (2). In typical sparse-neighborhood graph construction, k_g is expected to be smaller than n and is upper bounded by $n - 1$. Let m be the number of stable leaf balls, denoted by $\{B_1^*, \dots, B_m^*\}$, and let V_T be the set of tree nodes whose local MDL decisions are evaluated.

The preliminary stage includes data normalization, nearest-neighbor search, local-scale estimation, and reciprocal graph construction. Normalization requires $O(nd)$ time. For a general dense dataset, exact k_g -nearest-neighbor search has worst-case time complexity $O(n^2d)$. After the directed neighborhood relations are obtained, local-scale estimation, sparse affinity computation, and reciprocal-edge extraction are all performed on the k_g -nearest-neighbor support, requiring $O(nk_g)$ time and memory. Therefore, the preliminary graph construction costs

$$T_{\text{graph}} = O(n^2d + nk_g). \quad (33)$$

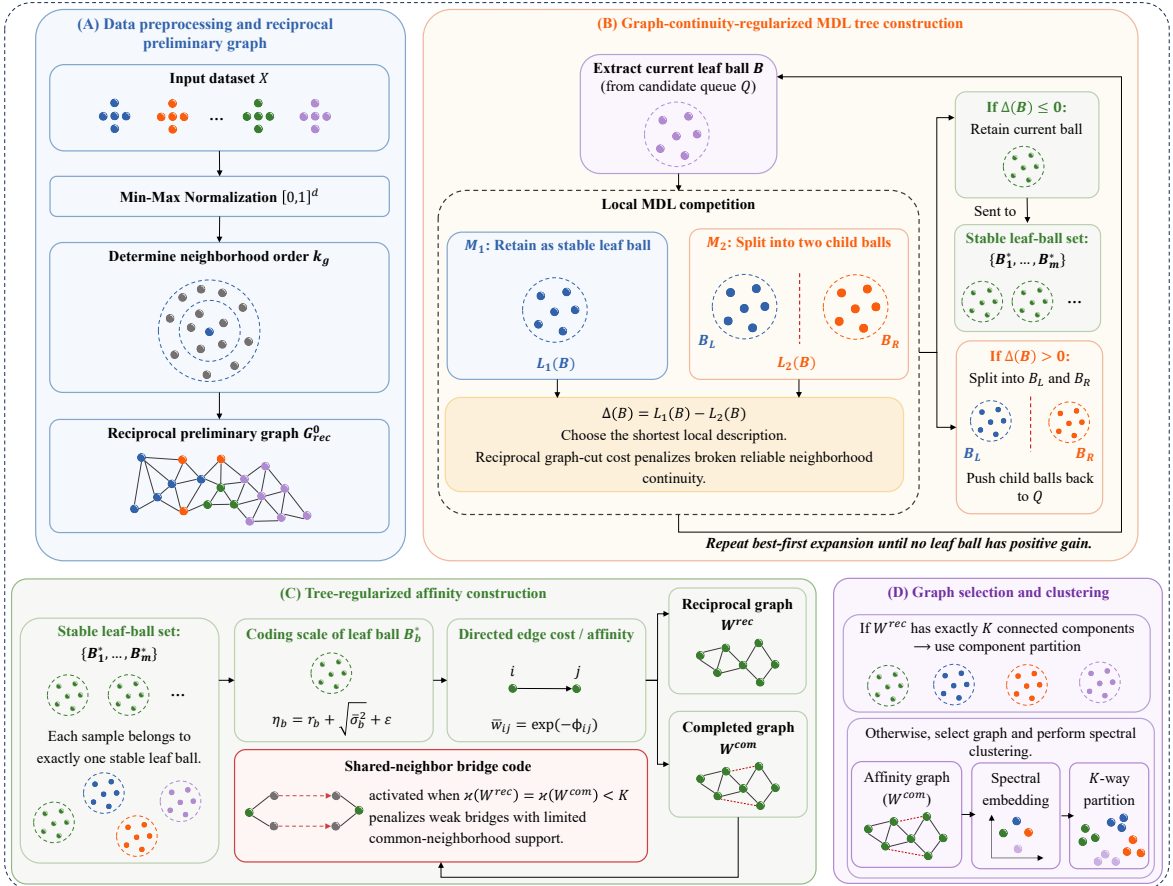


Figure 1: Framework of the proposed MDL-GBTRSC method. (A) Data preprocessing and reciprocal preliminary graph construction. (B) Graph-continuity-regularized MDL granular-ball tree construction, where each current leaf ball is locally evaluated by the retain model and the split model. (C) Tree-regularized affinity construction, where stable leaf balls provide coding-scale information and the shared-neighbor bridge code adjusts weak bridge relations. (D) Graph selection and clustering, where the final labels are obtained from connected components or spectral clustering on the selected graph.

The main additional cost comes from MDL-based granular-ball tree construction. For a current ball B with n_B samples, computing the isotropic code requires $O(n_B d)$ time. When the subspace-adaptive code is evaluated, the cost depends on the relative size of n_B and d . If $d \leq n_B$, the local scatter matrix is of size $d \times d$, and the cost of evaluating the leaf-ball code is

$$T_{\text{leaf}}(B) = O(n_B d^2 + d^3). \quad (34)$$

If $d > n_B$, the computation can be carried out through an $n_B \times n_B$ Gram matrix, giving

$$T_{\text{leaf}}(B) = O(n_B^2 d + n_B^3). \quad (35)$$

For one-dimensional data, only the isotropic code is needed, and the above bound reduces to the corresponding lower-dimensional case.

For split evaluation, samples in B are sorted according to a finite number of deterministic candidate orderings. Since Q_B already denotes the set of admissible ordering-position pairs, sorting, prefix-statistic construction, and scanning admissible cut positions require $O(n_B \log n_B + n_B d + |Q_B|d)$ time. The reciprocal graph-cut code in Eq. (21) is evaluated on the sparse neighborhood support, which costs $O(n_B k_g)$ for a ball B .

Algorithm 1: MDL-GBTRSC

Input: Dataset $X = \{x_i\}_{i=1}^n \subset \mathbb{R}^d$; optional cluster number K
Output: Cluster labels \hat{y}

- 1 Normalize X by Eq. (1);
- 2 Determine the neighborhood order k_g by Eq. (2);
- 3 Construct the reciprocal preliminary graph G_{rec}^0 ;
- 4 Estimate the finite-resolution variance floor σ_{min}^2 by Eq. (6);
- 5 Initialize the granular-ball tree with the root ball containing all samples;
- 6 **while** *there exists a leaf ball with positive MDL gain* **do**
- 7 Select the leaf ball B with the largest positive gain $\Delta(B)$;
- 8 Split B by the best generated admissible MDL split regularized by G_{rec}^0 ;
- 9 Update the tree and the MDL gains of the newly generated leaf balls;
- 10 **end**
- 11 Collect the stable leaf balls $\{B_1^*, \dots, B_m^*\}$;
- 12 Construct W^{rec} and W^{com} from the tree-regularized affinities, including the bridge adjustment when Eq. (27) holds;
- 13 **if** K is specified and W^{rec} contains exactly K connected components **then**
- 14 Set $W \leftarrow W^{\text{rec}}$;
- 15 **else**
- 16 Set $W \leftarrow W^{\text{com}}$;
- 17 **end**
- 18 **if** K is not specified **then**
- 19 Estimate K from the eigengap of L_{sym} ;
- 20 **end**
- 21 **if** W contains exactly K connected components **then**
- 22 Set \hat{y} as the connected-component labels of W ;
- 23 **else**
- 24 **if** W is disconnected and contains fewer than K connected components **then**
- 25 Allocate component-wise cluster numbers by Eq. (32);
- 26 Perform spectral clustering within each connected component;
- 27 **else**
- 28 Perform spectral clustering on W ;
- 29 **end**
- 30 **end**
- 31 **return** \hat{y} ;

Only a finite set of generated admissible split candidates is evaluated by the full split code. Let ρ_B be the number of such candidates. In the adopted deterministic candidate generation procedure, it satisfies

$$\rho_B \leq \min \{ |Q_B|, \max(2, \lceil \sqrt{n_B} \rceil) \}. \quad (36)$$

For the s -th generated split candidate, denote the two child balls by $B_{s,L}$ and $B_{s,R}$. The split-evaluation cost for B can be written as

$$T_{\text{split}}(B) = O \left(n_B \log n_B + n_B d + |Q_B| d + n_B k_g + \sum_{s=1}^{\rho_B} [T_{\text{leaf}}(B_{s,L}) + T_{\text{leaf}}(B_{s,R})] \right). \quad (37)$$

The tree is expanded in a best-first manner. Each accepted split increases the number of leaf balls by one. Therefore, if the final number of stable leaf balls is m , the number of accepted splits is $m - 1$, and the number of generated tree nodes is $O(m)$. The total cost of tree construction is

$$T_{\text{tree}} = O\left(\sum_{B \in V_T} T_{\text{split}}(B) + |V_T| \log |V_T|\right), \quad (38)$$

where the logarithmic term comes from best-first selection. This bound depends on the shape of the learned tree. A balanced tree leads to a smaller accumulated node size, whereas a highly skewed tree gives a looser worst-case bound.

After the tree is obtained, each sample is assigned to one stable leaf ball. The tree-regularized affinities are computed on the same sparse k_g -nearest-neighbor support. Computing the directed affinities and constructing the reciprocal and completed graphs therefore require $O(nk_g)$ time and memory. If the bridge adjustment is activated, common-neighborhood support is evaluated on sparse directed edges, adding $O(nk_g^2)$ time. Hence,

$$T_{\text{reg}} = O(nk_g + \delta_{\text{br}}nk_g^2), \quad M_{\text{reg}} = O(nk_g), \quad (39)$$

where δ_{br} is determined by Eq. (27).

The final partitioning cost depends on the component structure of the selected graph. Checking connected components costs $O(n + nk_g)$. If the selected graph contains exactly K connected components, the component labels are used directly, and no eigendecomposition is required. Otherwise, spectral relaxation is performed. For a sparse graph with $O(nk_g)$ nonzero entries, computing K eigenvectors by an iterative sparse eigensolver can be expressed as

$$T_{\text{spec}} = O(I_{\text{eig}}K nk_g + nK^2), \quad (40)$$

where I_{eig} is the number of eigensolver iterations. The subsequent clustering or discretization step on the spectral embedding adds $O(I_{\text{km}}nK^2)$ time when k -means with I_{km} iterations is used.

If the selected graph is disconnected and contains c connected components with $1 < c < K$, component-wise spectral clustering is applied. Let the components be H_1, H_2, \dots, H_c , and let K_r^* be the number of clusters assigned to H_r by Eq. (32). The corresponding cost is

$$T_{\text{cw}} = \sum_{r=1}^c O(I_{\text{eig}}K_r^*|H_r|k_g + |H_r|(K_r^*)^2) + O\left(I_{\text{km}} \sum_{r=1}^c |H_r|(K_r^*)^2\right). \quad (41)$$

When the selected graph contains more than K connected components, the method applies spectral relaxation to obtain a K -way partition, and the cost is included in T_{spec} . In the dense worst case, spectral decomposition may require $O(n^3)$ time and $O(n^2)$ memory.

Combining the above parts, the total time complexity in the fixed- K setting can be summarized as

$$T_{\text{total}} = O(n^2d + nk_g) + T_{\text{tree}} + O(nk_g + \delta_{\text{br}}nk_g^2) + T_{\text{part}}, \quad (42)$$

where $T_{\text{part}} = O(n + nk_g)$ if component labels are directly used, $T_{\text{part}} = T_{\text{spec}} + O(I_{\text{km}}nK^2)$ if global spectral clustering is performed, and $T_{\text{part}} = T_{\text{cw}}$ if component-wise spectral clustering is applied.

The memory consumption is mainly determined by the data matrix, sparse neighborhood graphs, tree storage, and spectral embedding:

$$M_{\text{total}} = O(nd) + O(nk_g) + M_{\text{tree}} + M_{\text{part}}. \quad (43)$$

If each sample stores only its current leaf assignment and each tree node stores summary statistics, $M_{\text{tree}} = O(n + m)$. If sample indices are explicitly stored for generated tree nodes, the memory cost depends on the accumulated node sizes. The partitioning memory M_{part} is $O(n)$ when component labels are directly used, $O(nK)$ for sparse spectral embedding, and may become $O(n^2)$ under dense eigendecomposition.

Therefore, the main computational costs of MDL-GBTRSC come from nearest-neighbor construction, local MDL-based tree generation, and spectral relaxation when eigendecomposition is required.

4. Experiments

This section evaluates the proposed MDL-GBTRSC on both real benchmark datasets and synthetic datasets. The real benchmark datasets are used to examine the general applicability of the proposed method on data with different sample sizes, feature dimensions, and numbers of classes. The synthetic datasets are used to further evaluate its ability to handle non-convex structures, nested clusters, bridging structures, uneven cluster sizes, density sparsity, and noisy local distributions. In addition to quantitative comparisons, visualization results on the synthetic datasets are provided to illustrate the clustering structures obtained by different methods.

4.1. Experimental Settings

All experiments were conducted in Python 3.12 on a workstation equipped with an AMD Ryzen 9 8940HX CPU, an NVIDIA GeForce RTX 5070 Ti GPU with 12 GB VRAM, 32 GB RAM, and a 1 TB SSD, under the Windows 11 operating system. All methods were evaluated under the same software and hardware environment. The source code and datasets have been made publicly available at <https://github.com/AnonymousUser0816/MDL-GBTRSC>.

For all methods, the cluster number K was set to the ground-truth number of classes. The ground-truth labels were used only to specify K and to compute the evaluation metrics, and were not involved in the clustering process. To ensure a fair and reproducible comparison, each method used a fixed parameter configuration across all real and synthetic datasets. No dataset-specific parameter tuning was performed.

The compared methods include two classical spectral clustering baselines and four representative clustering methods. The baseline methods are spectral clustering with a k -nearest-neighbor graph, denoted as SC-kNN, and spectral clustering with an RBF affinity graph, denoted as SC-RBF. The compared methods include GBCT [19], MDMSC [23], GBSC [20], and GMM-SC [13]. For these methods, the parameter settings followed the recommended values reported in the corresponding original papers or their released implementations. For methods involving stochastic components in the adopted implementation, including SC-RBF, GBSC, and GMM-SC, the random seed was fixed to 0 for reproducibility.

The proposed MDL-GBTRSC is deterministic under the same input data and does not require manually specified method-specific hyperparameters apart from the given cluster number K . The parameter settings used in the experiments are summarized in Table 1.

Table 1: Parameter settings used in the experiments.

Method	Parameter setting
MDL-GBTRSC	No manually specified method-specific hyperparameter
SC-kNN	$n_{\text{neighbors}} = 10$
SC-RBF	$\gamma = 1.0$, random seed = 0
GBCT	percent_avg= 0.2, minimum_ball= 2
MDMSC	$\lambda_{\text{ratio}} = 1.5$, $\beta = 16$, $k = 4$
GBSC	deta= 0.1, random seed = 0
GMM-SC	$\tau = 0.8$, $M = 250$, $s = 15$, random seed = 0

Table 2: Dataset information and abbreviations.

Abbr.	DataSet	Samples	Features	Classes
BTissue	Breast Tissue	106	9	6
Iris	Iris	150	4	3
Wine	Wine	178	13	3
Seeds	Seeds	210	8	3
Glass	Glass Identification	214	9	6
Thyroid	New Thyroid	215	5	3
Libras	Libras	360	90	15
WDBC	Breast Cancer Wisconsin	569	30	2
Banknote	Banknote Authentication	1372	4	2
Segment	Image Segmentation	2310	19	7
Rice	Rice Cammeo and Osmancik	3810	7	2
PageBlocks	Page Blocks Classification	5473	10	5
Digits	Optical Handwritten Digits	5620	64	10
Landsat	Landsat Satellite	6435	36	6
Isolet	Isolet	7797	617	26
PenDigits	Pen-Based Digits	10992	16	10
Bean	Dry Bean	13611	16	7
HTRU2	HTRU2	17898	8	2

4.2. Evaluation Metrics

Two external clustering metrics are adopted: adjusted Rand index (ARI) and normalized mutual information (NMI). ARI measures the agreement between the predicted partition and the ground-truth partition while correcting for chance. NMI evaluates the shared information between the predicted labels and the ground-truth labels from an information-theoretic perspective. For both metrics, larger values indicate better clustering performance. The best result for each metric on each dataset is highlighted in bold.

4.3. Datasets

The real UCI benchmark datasets² used in the experiments are listed in Table 2. These datasets cover different data scales and feature dimensions. The number of samples ranges from 106 to 17,898, the number of features ranges from 4 to 617, and the number of classes ranges from 2 to 26. This setting allows the evaluation to reflect the behavior of each method under different sample sizes, dimensionalities, and class structures.

²<https://archive.ics.uci.edu/>

The synthetic datasets³⁴ are summarized in Table 3. Compared with real benchmark datasets, synthetic datasets provide more explicit structural patterns, such as intertwined spiral structures, nested clusters, touching boundaries, bridging structures, uneven cluster sizes, and noisy distributions. Therefore, they are useful for examining whether the learned graph can preserve local connectivity and recover complex cluster shapes.

Table 3: Details of the synthetic datasets.

DataSet	Samples	Features	Classes	Main challenge
zelnik6	238	2	3	nested clusters, non-convex structure
zelnik1	299	2	3	nested clusters, non-convex structure
blobs	300	2	3	overlapping Gaussian-like clusters
zelnik2	303	2	3	uneven cluster sizes, background cluster
3-spiral	312	2	3	intertwined spiral structure, non-convex clusters
db2	315	2	4	nonlinear separability, shape diversity
jain	373	2	2	density sparsity, non-convex structure
zelnik4	622	2	5	uneven cluster sizes, background cluster
target	770	2	6	nested clusters, uneven cluster sizes, non-convex structure
aggregation	788	2	7	touching boundaries, bridging structures, shape diversity
chainlink	1000	3	2	nonlinear separability, non-convex structure
fourty	1000	2	40	many Gaussian-like clusters
wingnut	1016	2	2	sparse density distribution
N	1016	2	4	nested clusters, non-convex structure
A	1735	2	2	nonlinear separability, shape diversity
complex8	2551	2	8	nonlinear separability, shape diversity
diamond9	3000	2	9	touching boundaries, overlapping clusters
cure-t2-4k	4200	2	7	noise contamination, bridging structures, uneven cluster sizes
banana	4811	2	2	banana-shaped clusters, nonlinear separability
cluto-t8-8k	8000	2	9	noise contamination, nonlinear separability, shape diversity

4.4. Results on Real Benchmark Datasets

Table 4 reports the ARI and NMI results on the real benchmark datasets. Overall, MDL-GBTRSC achieves the best average performance among all compared methods, with an average ARI of 0.5910 and an average NMI of 0.6419. The second-best average ARI and NMI are obtained by MDMSC, with values of 0.5114 and 0.5806, respectively. This result shows that MDL-GBTRSC provides the best overall performance under the adopted fixed-configuration protocol.

On several datasets, including Iris, Wine, Glass, Thyroid, Banknote, Segment, and Landsat, MDL-GBTRSC obtains the best result on at least one of the two metrics. In particular, on Banknote, MDL-GBTRSC clearly outperforms the baseline and compared methods in both ARI and NMI. This suggests that directly constructing an affinity graph from a fixed pairwise rule may be insufficient when local neighborhood relations are ambiguous, whereas the MDL-induced granular-ball tree can provide useful local structural information for graph construction.

The results also show that no method dominates all datasets. SC-kNN obtains strong results on WDBC, Rice, Digits, Isolet, and PenDigits, while GBSC performs well on Bean and HTRU2. Such behavior is expected because real datasets may contain different local geometries, density distributions, and feature relevance patterns. Nevertheless,

³<https://github.com/milaan9/Clustering-Datasets/tree/master>

⁴<https://github.com/wyldbthxbw/GBC>

Table 4: Dataset-level comparison of ARI and NMI on the real benchmark datasets.

DataSet	Metric	Ours	Baseline		GBCT (TNNLS 2025)	MDMSC (AAAI 2025)	GBSC (TKDE 2023)	GMM-SC (TNNLS 2025)
			SC-kNN	SC-RBF				
BTissue	ARI	0.3718	0.3231	0.2973	0.0135	0.3334	0.3920	0.3207
	NMI	0.5207	0.4806	0.5202	0.2529	0.5183	0.5130	0.5359
Iris	ARI	0.9038	0.7445	0.6207	0.5681	0.9038	0.6537	0.9037
	NMI	0.8851	0.7777	0.6448	0.7337	0.8851	0.7490	0.8801
Wine	ARI	0.9309	0.8685	0.9149	0.7033	0.7414	0.5522	0.8537
	NMI	0.9088	0.8529	0.8926	0.7397	0.7528	0.6430	0.8417
Seeds	ARI	0.6896	0.6818	0.7338	0.1614	0.7664	0.7338	0.5881
	NMI	0.6696	0.6645	0.7025	0.3061	0.7343	0.7069	0.6231
Glass	ARI	0.2207	0.2189	0.1705	0.0396	0.1651	0.1420	0.1752
	NMI	0.3939	0.3601	0.3319	0.1608	0.3595	0.2796	0.3201
Thyroid	ARI	0.8273	0.2104	0.6592	0.4121	0.7997	0.7022	0.8019
	NMI	0.7574	0.3107	0.6245	0.4466	0.7219	0.7082	0.7131
Libras	ARI	0.3293	0.3526	0.2986	0.0930	0.3503	0.1023	0.3114
	NMI	0.6151	0.6170	0.5907	0.3096	0.6339	0.3400	0.5945
WDBC	ARI	0.7735	0.8115	0.6933	-0.0302	0.7423	0.7243	0.6823
	NMI	0.6670	0.7101	0.6143	0.0553	0.6410	0.6106	0.5696
Banknote	ARI	0.6011	-0.0032	0.0523	-0.0050	0.0009	0.0268	-0.0015
	NMI	0.5567	0.0140	0.0379	0.0068	0.0001	0.0797	0.0018
Segment	ARI	0.5062	0.4808	0.4268	0.3747	0.0811	0.4867	0.5015
	NMI	0.6619	0.6813	0.5816	0.5732	0.3338	0.6221	0.6212
Rice	ARI	0.6920	0.6981	0.6781	-0.0021	0.6753	0.6824	0.4954
	NMI	0.5791	0.5854	0.5643	0.0052	0.5709	0.5694	0.4229
PageBlocks	ARI	0.2908	0.0660	0.0903	0.4575	0.2251	0.2673	0.0660
	NMI	0.2342	0.1308	0.1181	0.2661	0.2066	0.1690	0.1308
Digits	ARI	0.8043	0.8358	0.6246	0.0003	0.8333	0.2864	0.6472
	NMI	0.8624	0.8956	0.7738	0.0426	0.9029	0.4604	0.7287
Landsat	ARI	0.5893	0.5537	0.5260	0.0005	0.5599	0.4826	0.4453
	NMI	0.6723	0.6546	0.5991	0.0100	0.6567	0.5767	0.5444
Isolet	ARI	0.4834	0.4874	0.2062	0.0078	0.4599	0.1532	0.4606
	NMI	0.7498	0.7712	0.6193	0.2159	0.7600	0.4299	0.7003
PenDigits	ARI	0.5805	0.5839	0.4908	0.0014	0.4107	0.4248	0.5486
	NMI	0.7923	0.7823	0.6741	0.0775	0.7001	0.5967	0.6878
Bean	ARI	0.5599	0.6295	0.4592	0.0978	0.6303	0.6679	0.6017
	NMI	0.6930	0.7326	0.5756	0.1868	0.7329	0.7274	0.7054
HTRU2	ARI	0.4838	0.4854	0.5406	0.0324	0.5272	0.6048	0.4636
	NMI	0.3342	0.3354	0.3575	0.0277	0.3406	0.3970	0.3098
Average	ARI	0.5910	0.5016	0.4713	0.1626	0.5114	0.4492	0.4925
	NMI	0.6419	0.5754	0.5457	0.2454	0.5806	0.5099	0.5517

MDL-GBTRSC achieves the highest average ARI and NMI across the tested real benchmark datasets, indicating good overall robustness under fixed parameter settings.

4.5. Results on Synthetic Datasets

Table 5 presents the ARI and NMI results on the synthetic datasets. MDL-GBTRSC achieves the best average performance, with an average ARI of 0.9568 and an average NMI of 0.9639. These results are higher than those of the compared methods under the same fixed-configuration protocol.

MDL-GBTRSC obtains perfect or near-perfect results on many datasets with explicit nonlinear structures, such as 3-spiral, chainlink, jain, target, wingnut, zelnik1,

Table 5: Dataset-level comparison of ARI and NMI on the synthetic datasets.

DataSet	Metric	Ours	Baseline		GBCT (TNNLS 2025)	MDMSC (AAAI 2025)	GBSC (TKDE 2023)	GMM-SC (TNNLS 2025)
			SC-kNN	SC-RBF				
zelnik6	ARI	1.0000	0.4720	0.6738	0.6463	0.6819	0.6376	0.7079
	NMI	1.0000	0.5064	0.6598	0.6420	0.7001	0.6313	0.7033
zelnik1	ARI	1.0000	1.0000	0.0376	0.5250	0.5386	0.5151	0.4993
	NMI	1.0000	1.0000	0.1493	0.6720	0.6885	0.6672	0.6441
blobs	ARI	0.9215	0.9126	0.8839	0.0056	0.8547	0.7889	0.7410
	NMI	0.8853	0.8760	0.8411	0.1025	0.8167	0.7811	0.7150
zelnik2	ARI	0.9901	0.5774	0.4937	0.0010	0.4776	0.1718	0.4798
	NMI	0.9831	0.6270	0.5643	0.0719	0.5561	0.3464	0.5865
3-spiral	ARI	1.0000	0.0534	-0.0052	0.9352	1.0000	0.0040	0.0002
	NMI	1.0000	0.0555	0.0011	0.9164	1.0000	0.0116	0.0058
db2	ARI	1.0000	0.2321	0.2059	1.0000	0.9446	0.2377	0.2199
	NMI	1.0000	0.5197	0.4208	1.0000	0.9332	0.5227	0.4328
jain	ARI	1.0000	0.4417	0.5612	0.2563	-0.0666	0.2563	-0.0487
	NMI	1.0000	0.4589	0.5365	0.2463	0.0530	0.2463	0.1695
zelnik4	ARI	0.9920	0.6363	0.6925	0.6478	0.6555	0.4883	0.9835
	NMI	0.9897	0.7286	0.7499	0.7208	0.7524	0.6315	0.9779
target	ARI	1.0000	0.3838	0.6350	0.6527	0.6688	0.0494	0.6706
	NMI	1.0000	0.5700	0.6364	0.6506	0.6659	0.1785	0.6825
aggregation	ARI	0.9869	0.4972	0.5637	0.7766	0.9761	0.8030	0.9219
	NMI	0.9824	0.7356	0.7396	0.8533	0.9726	0.8837	0.9196
chainlink	ARI	1.0000	1.0000	0.1244	1.0000	1.0000	0.0034	0.8279
	NMI	1.0000	1.0000	0.0925	1.0000	1.0000	0.0032	0.7782
fourty	ARI	1.0000	0.5947	0.3451	1.0000	0.9674	0.9546	0.9550
	NMI	1.0000	0.8881	0.7429	1.0000	0.9930	0.9865	0.9854
wingnut	ARI	1.0000	0.8305	0.4087	1.0000	1.0000	0.9456	0.3435
	NMI	1.0000	0.7385	0.3197	1.0000	1.0000	0.8951	0.2649
N	ARI	1.0000	0.5911	0.3835	1.0000	1.0000	0.6209	0.4903
	NMI	1.0000	0.7873	0.5477	1.0000	1.0000	0.7985	0.6499
A	ARI	1.0000	0.4247	0.3313	1.0000	1.0000	0.4973	0.3440
	NMI	1.0000	0.6764	0.5560	1.0000	1.0000	0.7187	0.5849
complex8	ARI	0.7318	0.7379	0.4073	0.5896	0.7796	0.5070	0.4980
	NMI	0.8277	0.8407	0.6182	0.7920	0.8564	0.7033	0.6840
diamond9	ARI	0.9992	0.9985	0.7428	0.8758	0.8657	0.9873	0.8064
	NMI	0.9990	0.9981	0.8316	0.9473	0.9381	0.9844	0.8925
cure-t2-4k	ARI	0.9161	0.6742	0.4467	0.64	0.2556	0.5287	0.5474
	NMI	0.8932	0.8263	0.6758	0.6916	0.4252	0.7454	0.7650
banana	ARI	1.0000	1.0000	0.3756	0.4879	0.9892	1.0000	0.2258
	NMI	1.0000	1.0000	0.2906	0.3890	0.9757	1.0000	0.1694
cluto-t8-8k	ARI	0.5991	0.5965	0.3940	0.5886	0.5063	0.5655	0.4695
	NMI	0.7183	0.7179	0.5701	0.7555	0.6623	0.6977	0.6453
Average	ARI	0.9568	0.6327	0.4351	0.6814	0.7547	0.5281	0.5342
	NMI	0.9639	0.7276	0.5272	0.7226	0.7995	0.6217	0.6128

zelnik2, zelnik4, zelnik6, db2, banana, A, and N. These datasets are challenging because samples from different clusters may be locally close, while samples from the same cluster may be globally far apart. The strong performance of MDL-GBTRSC indicates that the graph-continuity regularized tree construction can preserve meaningful local connectivity and reduce inappropriate fragmentation.

For datasets involving touching boundaries, bridging structures, uneven cluster sizes, or noise, such as aggregation, cure-t2-4k, diamond9, and cluto-t8-8k, MDL-GBTRSC

also achieves competitive or best performance. These results suggest that stable leaf balls provide useful local coding-scale information for the final affinity graph. Compared with a graph constructed only from fixed pairwise affinities, the tree-regularized graph can better adapt to heterogeneous local structures.

It is also observed that MDMSC obtains the best results on complex8, and several methods obtain tied perfect performance on some relatively clear synthetic structures. This indicates that the advantage of MDL-GBTRSC is reflected not in a single special case, but in its overall behavior across diverse structural patterns. Under the fixed-configuration protocol, MDL-GBTRSC maintains the best average ARI and NMI, showing its robustness on synthetic structural benchmarks.

4.6. Visualization Analysis on Synthetic Datasets

To further examine the structural recovery ability of MDL-GBTRSC, Fig. 2 presents the visualization results of the proposed method on the 20 synthetic datasets. These visualizations complement the quantitative results in Table 5 by showing how MDL-GBTRSC partitions datasets with different geometric structures. Complete visualization results of the compared algorithms are provided in Appendix A.

For non-convex datasets such as 3-spiral and banana, the proposed method can preserve the continuity of curved or manifold-like clusters. This is consistent with the design of MDL-GBTRSC, where the preliminary graph provides local connectivity information during tree construction, and the stable leaf balls further provide local coding scales for the final affinity graph.

For nested or uneven-sized structures, such as target, N, zelnik1, and zelnik4, the visualization results show that MDL-GBTRSC can maintain the separation between inner and outer structures or between clusters with different sizes. This indicates that the local description-length comparison helps reduce the dependence on a single global scale.

For datasets with touching boundaries or bridging effects, such as aggregation and cure-t2-4k, the visualization results further show that MDL-GBTRSC can reduce misleading cross-cluster connections while preserving meaningful within-cluster continuity. By evaluating candidate splits according to both description-length reduction and graph-continuity cost, the learned tree-regularized graph can better reflect local structural relations before spectral partitioning.

4.7. Runtime Comparison

In addition to clustering accuracy, runtime is evaluated on the real benchmark datasets. Fig. 3 shows the runtime of different algorithms on each dataset. Since the running times vary over several orders of magnitude, the vertical axis is shown in logarithmic scale. Table 6 reports the average runtime of each algorithm over the 18 real benchmark datasets.

As shown in Table 6, SC-kNN has the shortest average runtime, followed by GBSC and GMM-SC. MDL-GBTRSC requires more time than these lightweight methods because it includes preliminary neighborhood graph construction and MDL-based granular-ball tree generation before the final spectral partition. These additional computations are used to introduce local structural information into the affinity graph. Therefore, the runtime of MDL-GBTRSC reflects the cost of constructing a more structured graph representation.

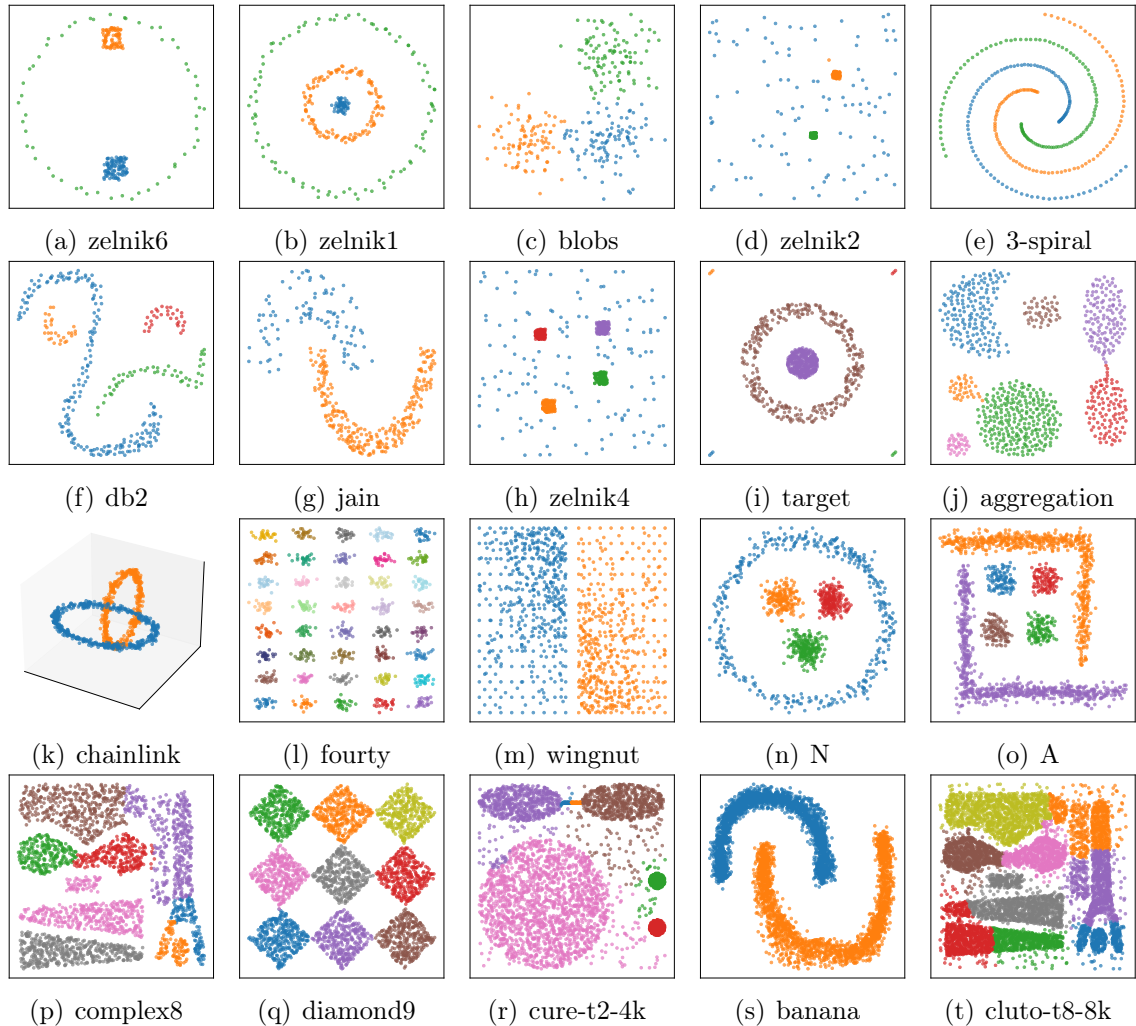


Figure 2: Visualization results of MDL-GBTRSC on the 20 synthetic datasets.

Table 6: Average runtime of different algorithms on the real benchmark datasets.

Method	Average runtime (s)	Rank
SC-kNN	4.2193	1
GBSC	5.6863	2
GMM-SC	6.8699	3
MDMSC	12.8633	4
MDL-GBTRSC	22.0379	5
GBCT	28.6099	6
SC-RBF	47.1798	7

At the same time, MDL-GBTRSC is faster on average than GBCT and SC-RBF. The runtime of SC-RBF increases substantially on high-dimensional datasets such as Isolet, where dense affinity construction becomes costly. GBCT also shows a relatively high average runtime on the tested real datasets. In contrast, MDL-GBTRSC achieves the best average ARI and NMI in Table 4 with an intermediate average runtime. These results indicate that the proposed method provides a reasonable balance between clustering performance and computational cost under the adopted

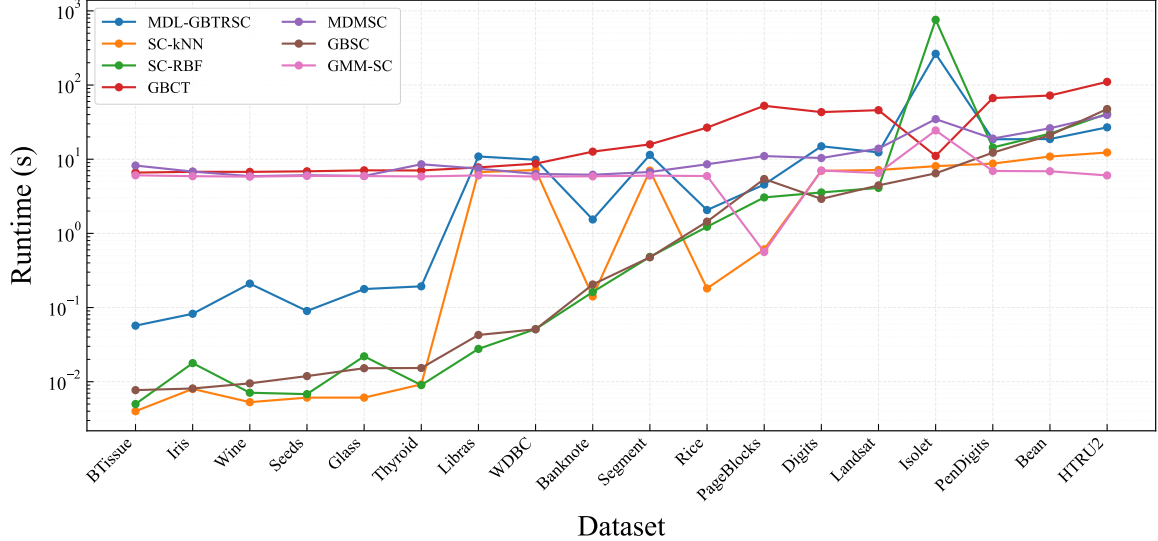


Figure 3: Runtime comparison of different algorithms on the real benchmark datasets.

experimental protocol.

5. Discussion and Conclusions

This paper proposed MDL-GBTRSC, a Minimum Description Length based Granular-Ball Tree-Regularized Spectral Clustering method. The method uses MDL to construct a granular-ball tree and then incorporates the stable leaf balls into the construction of the sample-level affinity graph. Different from methods that use granular balls mainly as reduced graph nodes or anchors, MDL-GBTRSC keeps the final graph at the sample level. The learned leaf balls provide local coding-scale information, while reciprocal neighborhood relations are used to preserve local continuity during tree construction.

The experimental results on the real benchmark datasets show that MDL-GBTRSC obtains the highest average ARI and NMI among the compared methods under the adopted fixed-configuration protocol. This result suggests that the MDL-induced granular-ball tree can provide useful local structural information for affinity graph construction. The dataset-level results also show that the performance varies across datasets. For example, SC-kNN performs well on several real datasets, and GBSC obtains better results on some datasets. This indicates that different clustering methods may be favored by different data geometries, density distributions, and feature characteristics. Nevertheless, the average results show that MDL-GBTRSC has good overall performance across the tested real benchmark datasets.

The results on the synthetic datasets further illustrate the role of tree-regularized graph construction. These datasets contain non-convex, nested, curved, bridging, noisy, and unevenly distributed structures. MDL-GBTRSC achieves the highest average ARI and NMI on these datasets, indicating that the proposed graph construction can preserve local continuity in many structurally complex cases. The visualization results provide a complementary view of this behavior. On several non-convex or nested datasets, the learned graph helps maintain within-cluster connectivity and reduces inappropriate merging between nearby but structurally different regions. This observation is consistent with the design of the method: reciprocal neighborhood

continuity guides local tree construction, and stable leaf balls provide local coding scales for the final graph.

The runtime comparison shows that MDL-GBTRSC is not the fastest method. It requires more time than lightweight methods such as SC-kNN, GBSC, and GMM-SC, mainly because it includes preliminary neighborhood graph construction and MDL-based granular-ball tree generation before spectral partitioning. This additional cost is related to the use of local model comparison and tree-regularized graph construction. At the same time, MDL-GBTRSC is faster on average than GBCT and SC-RBF on the tested real datasets. Therefore, the proposed method should be viewed as a clustering-quality-oriented method rather than a purely efficiency-oriented variant of spectral clustering. Under the current experimental setting, it provides a reasonable balance between clustering performance and computational cost.

There are still several aspects that require further study. First, although MDL-GBTRSC avoids manually tuned method-specific hyperparameters apart from the given cluster number, its computational cost is higher than that of simple graph construction methods. For larger datasets, approximate nearest-neighbor search, parallel MDL evaluation, and more efficient candidate split evaluation may be needed. Second, the method still relies on local neighborhood relations. If the initial neighborhood graph is strongly affected by high-dimensional noise, severe overlap, or weak cluster separability, the resulting tree and final graph may also be affected. Third, the experiments mainly follow the common external evaluation setting in which the true number of clusters is given. Although an eigengap-based rule is included when K is unspecified, automatic cluster-number estimation deserves more systematic evaluation.

Future work will focus on improving efficiency and robustness. More efficient implementations can be developed by using approximate graph construction, compact ball indexing, and parallel local MDL computation. It is also worth extending the current framework to high-dimensional feature selection, streaming data, and incremental clustering, where both the granular-ball tree and the affinity graph may need to be updated dynamically. In addition, the idea of using MDL-induced local structures to regularize graph construction may be applied to other graph-based learning tasks.

In conclusion, MDL-GBTRSC connects local granular-ball representation and spectral graph construction within an MDL-based framework. By using reciprocal neighborhood continuity in tree construction and stable leaf-ball coding scales in graph construction, the proposed method provides an interpretable way to regularize the affinity graph used for spectral clustering. Experiments on real and synthetic datasets show that this design can improve overall clustering performance, especially on datasets where local structure plays an important role.

CRedit authorship contribution statement

Zeqiang Xian: Conceptualization, Methodology, Writing – original draft, Software, Validation. **Caihui Liu:** Conceptualization, Methodology, Writing – review & editing, Validation, Supervision. **Yong Zhang:** Software, Data curation. **Wenjing Qiu:** Software, Data curation.

Declaration of Competing Interest

The authors declare that they have no known competing financial interests or personal relationships that could have appeared to influence the work reported in this

paper.

Data availability

Data will be made available on request.

Acknowledgment

The research is supported by the National Natural Science Foundation of China under Grant No. 62566003, Graduate Innovation Funding Program of Jiangxi Province under Grant No. YC2025-S224.

References

- [1] L. Hu, M. Jiang, J. Dong, X. Liu, Z. He, Interpretable clustering: A survey, *ACM Computing Surveys* 58 (8) (2026) 1–21.
- [2] U. Von Luxburg, A tutorial on spectral clustering, *Statistics and computing* 17 (4) (2007) 395–416.
- [3] A. Ng, M. Jordan, Y. Weiss, On spectral clustering: Analysis and an algorithm, *Advances in neural information processing systems* 14 (2001).
- [4] L. Ding, C. Li, D. Jin, S. Ding, Survey of spectral clustering based on graph theory, *Pattern Recognition* 151 (2024) 110366.
- [5] K. Berahmand, F. Saberi-Movahed, R. Sheikhpour, Y. Li, M. Jalili, A comprehensive survey on spectral clustering with graph structure learning, *arXiv preprint arXiv:2501.13597* (2025).
- [6] L. Kong, J. Xue, F. Nie, X. Li, Direct spectral clustering with new graph learning for better fitting, *IEEE Transactions on Knowledge and Data Engineering* 37 (7) (2025) 3991–4002.
- [7] N. Wang, Z. Cui, A. Li, Y. Lu, R. Wang, F. Nie, Structured doubly stochastic graph-based clustering, *IEEE Transactions on Neural Networks and Learning Systems* 36 (6) (2025) 11064–11077.
- [8] J. Li, F. Qi, H. Yuan, C. Zhong, H. Cai, Stacked network to realize spectral clustering with adaptive graph learning, *IEEE Transactions on Knowledge and Data Engineering* 36 (7) (2023) 3501–3513.
- [9] X. Yang, M. Zhu, Y. Cai, Z. Wang, F. Nie, Fast spectral clustering with self-adapted bipartite graph learning, *Information Sciences* 644 (2023) 118810.
- [10] R. Wang, H. Chen, Y. Lu, Q. Zhang, F. Nie, X. Li, Discrete and balanced spectral clustering with scalability, *IEEE Transactions on Pattern Analysis and Machine Intelligence* 45 (12) (2023) 14321–14336.
- [11] C. Gao, W. Chen, F. Nie, W. Yu, Z. Wang, Spectral clustering with linear embedding: A discrete clustering method for large-scale data, *Pattern Recognition* 151 (2024) 110396.

- [12] J. Zhou, X. Zhang, C. Gao, Z. Lai, W. Pedrycz, Efficient spectral embedding representation approximation for large-scale data clustering, *Pattern Recognition* (2025) 112693.
- [13] W. Zhang, J. Zhao, L. Yu, S. Wang, Gmm enhanced anchor-based spectral clustering for large-scale data, *IEEE Transactions on Neural Networks and Learning Systems* 36 (10) (2025) 18089–18103.
- [14] N. Naseri, M. Eftekhari, F. Saberi-Movahed, M. Radjabalipour, L. A. Belanche, A similarity measure based on subspace distance for spectral clustering, *Neurocomputing* 620 (2025) 129187.
- [15] Y. Zhu, Q. Li, W. Liu, C. Yin, Diffusion process with structural changes for subspace clustering, *Pattern Recognition* 158 (2025) 111066.
- [16] G. Yue, A. Deng, Y. Qu, H. Cui, X. Wang, Stratified multi-density spectral clustering using gaussian mixture model, *Information Sciences* 633 (2023) 182–203.
- [17] S. Xia, G. Wang, X. Gao, X. Lian, Granular-ball computing: an efficient, robust, and interpretable adaptive multi-granularity representation and computation method, *arXiv preprint arXiv:2304.11171* (2023).
- [18] S. Xia, Y. Liu, X. Ding, G. Wang, H. Yu, Y. Luo, Granular ball computing classifiers for efficient, scalable and robust learning, *Information Sciences* 483 (2019) 136–152.
- [19] S. Xia, B. Shi, Y. Wang, J. Xie, G. Wang, X. Gao, Gbct: efficient and adaptive clustering via granular-ball computing for complex data, *IEEE Transactions on Neural Networks and Learning Systems* 36 (7) (2025) 12159–12172.
- [20] J. Xie, W. Kong, S. Xia, G. Wang, X. Gao, An efficient spectral clustering algorithm based on granular-ball, *IEEE Transactions on Knowledge and Data Engineering* 35 (9) (2023) 9743–9753.
- [21] D. Cheng, S. Liu, S. Xia, G. Wang, Granular-ball computing-based manifold clustering algorithms for ultra-scalable data, *Expert Systems with Applications* 247 (2024) 123313.
- [22] D. Cheng, X. Jiang, S. Xia, G. Wang, J. Huang, S. Zhang, Y. Wang, Fast spectral clustering via pseudo-label-based granular-ball division for large-scale data, *IEEE Transactions on Knowledge and Data Engineering* 38 (5) (2026) 2807–2817.
- [23] Z. Xu, Z. Long, H. Meng, Clustering by mining density distributions and splitting manifold structure, in: *Proceedings of the AAAI Conference on Artificial Intelligence*, Vol. 39, 2025, pp. 21842–21849.
- [24] Z. Xian, C. Liu, Y. Zhang, W. Qiu, D. Miao, W. Pedrycz, Mdl-gbg: A non-parametric and interpretable granular-ball generation method for clustering, *arXiv preprint arXiv:2605.08759* (2026).
- [25] Z. Xian, C. Liu, Y. Zhang, W. Qiu, D. Miao, W. Pedrycz, A boundary-aware non-parametric granular-ball classifier based on minimum description length, *arXiv preprint arXiv:2605.11406* (2026).

Appendix A. Complete Visualization Results of the Compared Algorithms

This appendix provides the complete visualization results of the compared algorithms on the 20 synthetic datasets. The visualization results of MDL-GBTRSC are shown in Fig. 2 in the main text. In Figs. A.4 and A.5, each row corresponds to one dataset and each column corresponds to one compared algorithm. From left to right, the six algorithms are SC-kNN, SC-RBF, GBCT, MDMSC, GBSC, and GMM-SC. The datasets are arranged in ascending order of sample size, consistent with Table 3. Colors denote the predicted cluster labels.

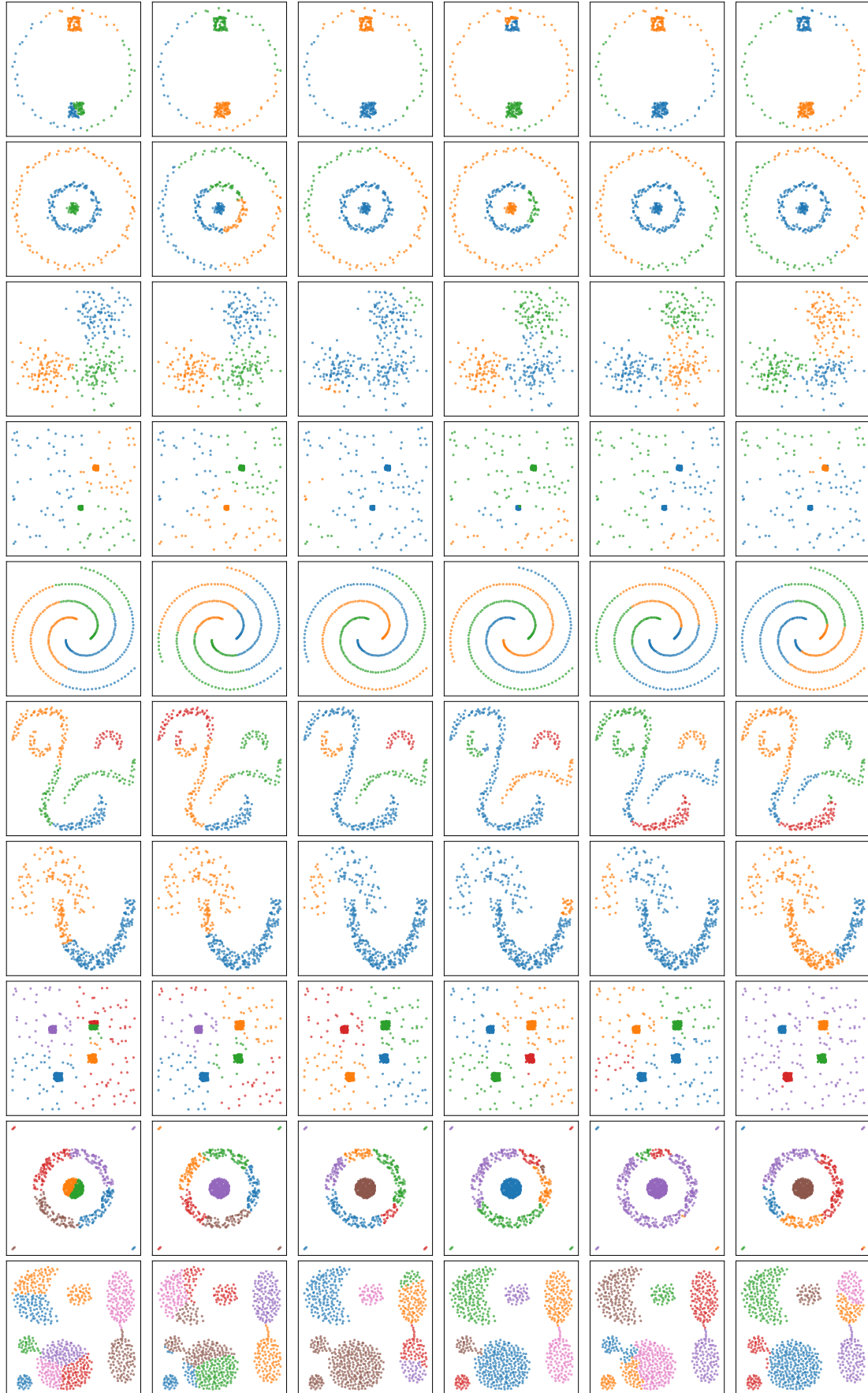


Figure A.4: Visualization results of the compared algorithms on the first ten synthetic datasets.

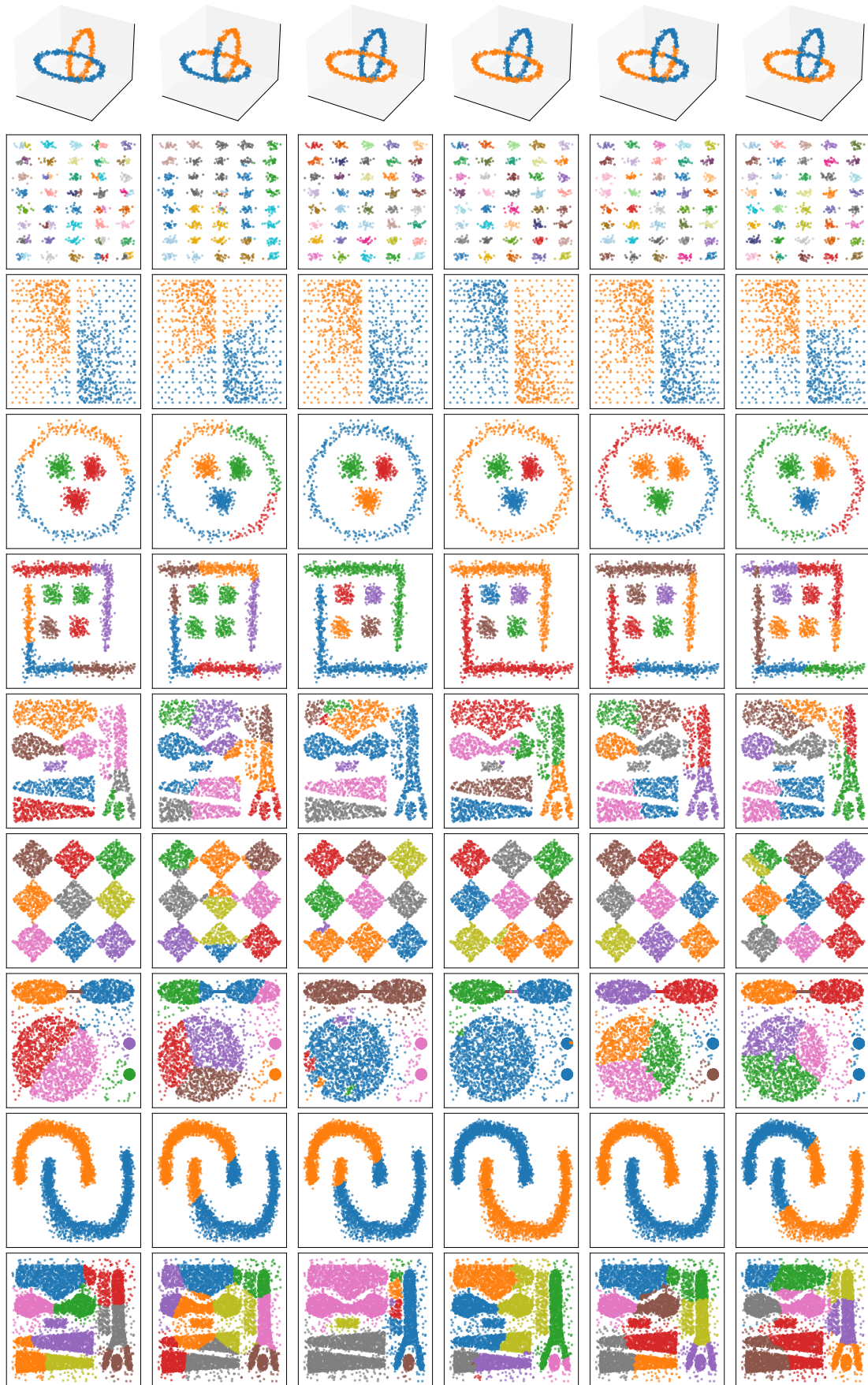


Figure A.5: Visualization results of the compared algorithms on the second ten synthetic datasets.